Phase transitions in the layered structure of diguanidinium tetraiodoplumbate

Marek Szafrański
Faculty of Physics, Adam Mickiewicz University, Umultowska 85, 61-614 Poznań, Poland

Andrzej Katrusiak
Faculty of Chemistry, Adam Mickiewicz University, Grunwaldzka 6, 60-780 Poznań, Poland
(Received 1 March 1999)

Sterical effects and the coupling between the cationic dynamics and the anionic-supralattice distortions lead to a series of phase transitions in the crystals of diguanidinium tetraiodoplumbate, $[C(NH_2)_3]_2^+ \cdot PbI_4^{2-}$. The crystals have been characterized by dielectric and calorimetric measurements at ambient and high hydrostatic pressures, as well as by single-crystal x-ray and neutron-powder diffraction at varied temperatures. At 287 K the crystal structure is monoclinic, but the strongly corrugated polyanionic sheets approximate the orthorhombic symmetry of the high-temperature phases. Guanidinium cations are enclosed in voids within the polyanions, and in channels between the neighboring sheets. At 0.1 MPa and 307 K the monoclinic phase undergoes a ferroelastic second-order transition to the orthorhombic phase, and at 356 K another continuous transition to the orthorhombic phase with the unit cell reduced four times in volume. The phase diagram reveals an unusual character of the pressure-induced transition with a critical point at 245 K and 270 MPa. Also a triple point at 358 K and 780 MPa has been detected. The mechanisms of the phase transitions have been postulated.

I. INTRODUCTION

The crystals of general formula A_2MX_4, where A is a molecular cation, M a divalent metal, and X a halogen, form various structures, mainly with anionic sublattices built of the MX_6 octahedra shearing faces, edges or corners. In the latter most common case the crystals have the layered-perovskite and perovskite-type structures, and are simple models of interionic and interlayer interactions, phase transitions, as well as of property-structure relations. In many respects they resemble transformations in three-dimensional ABO_3 perovskites, main components of the Earth crust, and in somewhat more complex high-temperature superconductors. The layered structures are low-dimensional analogues of epitaxial layers characterized by high layer homogeneity, and provide convenient objects for studying electronic and optical phenomena resulting from size-related quantum effects.[1–3] A characteristic feature of layered structures is a high susceptibility to thermodynamic parameters of temperature or pressure, disturbing the balance between interactions of the ions and the layers, and leading to phase transitions.

Owing to the simplicity of the A_2MX_4 structures, new materials can be engineered and their properties can be tuned by combining various layer and interlayer components.[3,4] The phase transitions in organic-based halogenometallates arise essentially from disordering conformation or orientation of the cations,[5] or from rotational distortions of the anionic sublattices.[6,7] The freezing of rotational modes of the MX_6 octahedra is responsible, among other factors, for ferroelectric properties and incommensurate modulations of the crystals from the BaMF$_4$ family,[8–10] where M is Mg, Mn, Fe, Co, Ni, Zn, etc. These compounds, particularly fluorine analogues of perovskites, were promising materials for fast electronic devices. The layered BaMF$_4$ compounds, where like in perovskites the phase transitions are connected with displacements of the octahedra, offer a simpler insight into the mechanism of the transformations due to their lower dimensionality.

A further extension of this series of transformable materials is presented in this report. Recently a new member of the A_2MX_4 family, diguanidinium tetraiodoplumbate, $[C(NH_2)_3]_2^+PbI_4^{2-}$ hereafter referred to as G_2PbI_4, with the anionic sublattice pattern identical to that in BaMF$_4$, was synthesized.[11] By increasing the size of the octahedral blocks building the polyanionic layers we managed to include two organic cations in the voids between the sheets, in one barium dication stead. This creates a new quality, because organic cations of diverse sizes and shapes may be introduced into the crystal, and transformations of such materials can be induced by various configurations of cationic orientations assumed in the lattice. The cations interact with their neighbors in the adjacent cavities, and additional interactions of the cations with the polyanionic sheets is prominent. These interactions can be modified and they change properties and the mechanisms of the phase transitions of the crystal, while the system preserves the simplicity of a layered structure. The structure of G_2PbI_4 offers a unique opportunity to study dynamics and transformations of strained organic monolayers, and to compare them with the analogous monolayers epitaxially grown on covalent or ionic matrices.

Previously reported calorimetric studies revealed a continuous phase transition in G_2PbI_4 at 307 K, associated with a transition entropy suggesting its order-disorder nature.[11] A possibility of an additional transformation near 170 K was indicated by proton NMR studies.[12] The results of structural, calorimetric, dielectric, dilatometric, and high-pressure measurements presented in this report clarify the phase relations and reveal an intriguing mechanism of the phase transitions in G_2PbI_4, which may be a common feature of many salts built of layered anionic frameworks containing organic cations.

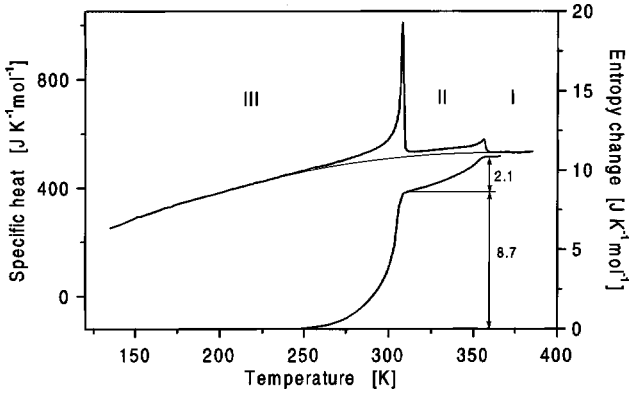

FIG. 1. Specific heat (upper curve) and transition entropies (lower curve) of G_2PbI_4. The phases are labeled by the Roman numbers indicated in the plot

II. EXPERIMENT

Specific heat measurements were performed by differential scanning calorimetry (DSC) on a Perkin-Elmer DSC-7 calorimeter. A polycrystalline sample of 47.7 mg was placed in a nonhermetic aluminum cell in the nitrogen atmosphere. Temperature was changed at a rate of 10 $\mathrm{K\,min^{-1}}$. The transition entropies were calculated from the $C_p(T)$ dependence. Magnitudes of total entropy gain are sensitive to the choice of the base line, and a proper estimation of the base line is the main difficulty when studying thermal anomalies stretching over a long range of temperatures. This was the case in G_2PbI_4, where overlapping signals of two phase transitions extend to over 110 K (Fig. 1). In order to determine the base line, the normal part of the temperature dependence of C_p, denoted C_p^0 was fitted by a polynomial and then extrapolated to the anomalous region. The uncertainty of ΔS determination estimated by probing alternative models reproducing the base line reaches 20%, much higher than the apparatus 2–3 % accuracy.

Dielectric measurements were performed with an impedance analyzer HP 4192A in the frequency range from 10 kHz to 13 MHz. The single crystals with golden electrodes deposited by evaporation on the surfaces perpendicular to the main crystallographic directions were analyzed. The electrode surfaces of the crystals cut perpendicular to axes *a* and *c* were of about 1 $\mathrm{mm^2}$, and of 6 $\mathrm{mm^2}$ perpendicular to *b*. Dielectric constant and tangent of dielectric losses were measured between 100 and 400 K, and the temperature was changed at the rate of 0.5 $\mathrm{K\,min^{-1}}$.

The influence of hydrostatic pressure on the G_2PbI_4 structure was studied by differential thermal analysis (DTA).[13] Helium and nitrogen were used alternatively as pressure transmitting media. A polycrystalline sample was encapsulated in an indium vessel. The measurements were performed under a pressure from 0.1 to 900 MPa and in the temperature range from 150 to 400 K. The temperature was changed at the rate of 2 $\mathrm{K\,min^{-1}}$. The transition temperatures used in the *p-T* phase diagram were determined on heating the sample as the onset or maximum of thermal anomaly, respectively, for the first-order and continuous phase transitions. The transitions temperatures were not corrected for the rates of temperature changes.

A KUMA-4 diffractometer equipped with a graphite monochromator was used for x-ray studies. The temperature was controled with a stream of air, and stabilized automatically within 0.5 deg. The unit-cell dimensions (Fig. 2) were obtained by least-squares fits to 40 automatically centered reflections. It was clearly established from the unit-cell dimensions and by comparing equivalent reflections in the Laue class *mmm*, that the crystals become orthorhombic above $T_2 = 307$ K. Intensity data were collected at 287 K. The θ-2θ scan mode at variable speed ranging from 1.0 to $30°\ \mathrm{min^{-1}}$ depending on reflection intensity was applied. Two control reflections measured every 200 current reflections showed no systematic change in their intensity throughout the data collections. The intensities were corrected for Lp effects and absorption. The structure of the low-temperature phase, denoted III, was solved by the Patterson method. After locating the Pb and I atoms, two guanidinium cations were located in ΔF maps. The geometry of the cations were constrained to the dimensions observed for strongly vibrating structures, C-N of 1.31 Å (Refs. 14 and 15) and N-H of 0.86 Å. The Pb and I atoms were refined with anisotropic temperature factors, while the C and N atoms with isotropic ones. Details of the data collection and structure refinement are given in Table I. The calculations were performed with program SHELXL,[16] atomic scattering factors were those incorporated in this program. The final atomic parameters are listed in Table II.

III. RESULTS

A. Specific heat between 135 and 385 K

Two thermal anomalies have been found in the temperature dependence of specific heat between 135 and 385 K (see the upper curve in Fig. 1). The jump in specific heat $\Delta C_{p2} = 0.583\ \mathrm{J\,g^{-1}\,K^{-1}}$ at $T_2 = 307$ K corresponds to the continuous phase transition observed earlier,[11] while the other jump $\Delta C_{p1} = 0.063\ \mathrm{J\,g^{-1}\,K^{-1}}$ marks a new phase transition at $T_1 = 356$ K. The high-temperature phase existing above 356 K will be referred to as phase I, the phase between 356 and 307 K as phase II, and the low-temperature phase as phase III.

The character of thermal anomalies, as well as no temperature hysteresis, are characteristic for continuous phase transitions. The anomalous parts of entropy ΔS due to the phase transitions as a function of temperature are given by the lower curve in Fig. 1. The transition at T_2 is accompanied by the total entropy gain $\Delta S_2 = 8.7\ \mathrm{J\,K^{-1}\,mol^{-1}}$, which corresponds to $R \ln 2.7$ (R is the gas constant) indicating that this phase transition has an order-disorder character. Taking into account the uncertainty in ΔS_2 (see Sec. II), the increase in the number of configurations in phase II can be estimated as between two and four times. Relatively small entropy change ΔS_1, of 2.1 $\mathrm{J\,K^{-1}\,mol^{-1}}$, indicates a displacive nature of the phase transition at T_1. In the low-temperature region below 200 K no anomalies in the $C_p(T)$ dependence could be ascribed to a phase transition proposed from solid-state ^{1}H-NMR at about 170 K.[12]

B. Dielectric properties

The character of changes in ε_a', ε_b', and ε_c' with temperature is similar, and illustrated by $\varepsilon_b'(T)$ shown in Fig. 3. A

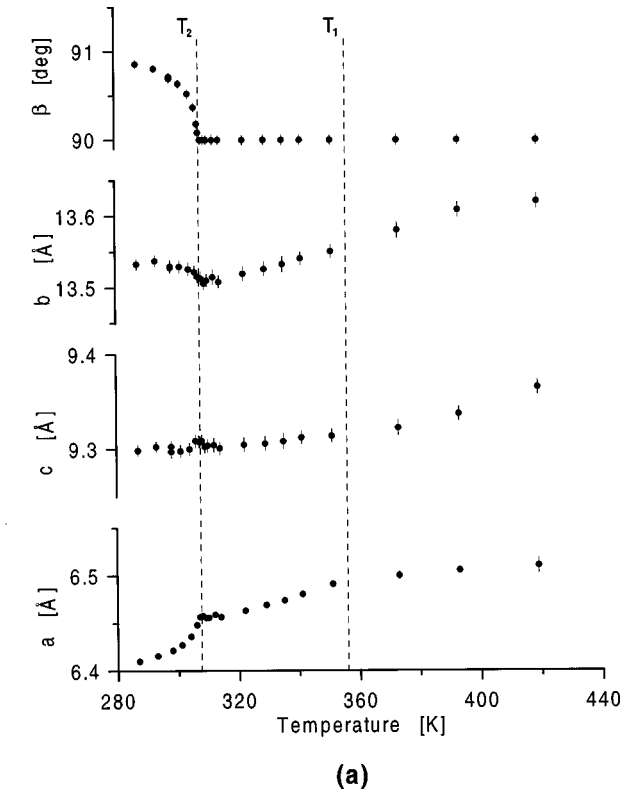

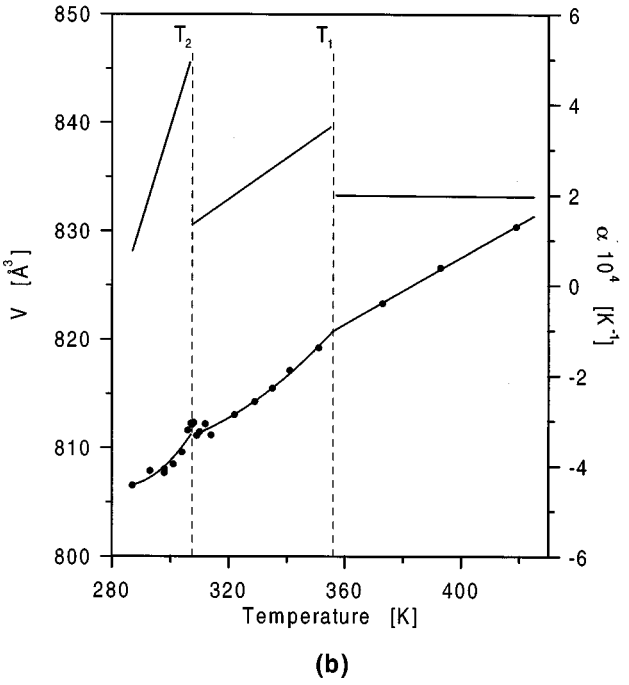

FIG. 2. Temperature dependence of unit-cell dimensions a,b,c,β (a), as well as of two G_2PbI_4 formula-units volume V (i.e., the unit-cell volume in phase I) and the volume thermal expansion coefficient α (b) between 280 and 420 K. For phases II and III, where parameters a and b are doubled compared to phase I, halves of these parameters have been plotted.

gradual anomalous increase in the dielectric constant is observed when T_2 is approached from the low-temperature side, while only a small anomaly marks the phase transition at T_1. No dielectric relaxation process was observed in the applied range of the measuring field frequencies.

TABLE I. Crystal data and structure refinement for G_2PbI_4 at 287 K.

Chemical formula	$[C(NH_2)_3]_2^- \cdot PbI_4^{2+}$
Wavelength	0.71069 Å
Crystallographic system	monoclinic
Space group	$P2_1/n$
Unit-cell dimensions	$a=12.831(2)$ Å
	$b=27.052(5)$ Å
	$c=9.298(1)$ Å
	$\beta=90.81(1)$ deg
Unit-cell volume	3227.0(8) Å^3
Z	8
Density (calculated)	3.437 Mg/m^3
Absorption coefficient	18.09 mm^{-1}
Crystal size	$0.01\times0.01\times0.03$ mm
Θ range for data collection	1.51–23.33 deg
Reflections collected	7645
Independent reflections	4520[$R_{int}=0.0708$]
Refinement method	Full-matrix least-squares on F^2
Data/restraints/parameters	4504/24/160
Goodness-of-fit on F^2	1.017
Final R indices [$I>2\sigma(I)$]	$R1=0.071, wR2=0.146$
Extinction coefficient	0.00028(14)

C. Temperature dependence of lattice dimensions

The continuous character of the phase transitions at T_1 and T_2 is consistent with the observed changes in the crystal unit cell parameters with temperature, shown in Fig. 2. The unit-cell dimensions a and b double when the crystal is cooled through T_1, however the crystal expansion hardly changes at T_1 for parameters b and c, and is best visible for parameter a. Much more profound anomalies are observed in the lattice parameters on heating the crystal through T_2. Apart from the spontaneous strain distorting angle β from 90°, strong anomalies appear in the temperature dependence of a and b. They cannot be ascribed to secondary effects following the monoclinic distortion, but they rather indicate a complex mechanism of the phase transition between the orthorhombic and monoclinic phases. As expected for continuous phase transitions, the crystal volume is weakly affected at T_1 and T_2. The temperature dependence of the unit-cell volume was fitted by polynomial functions separately for each of the phases, and then the coefficient of volume thermal expansion, α, was calculated [see Fig. 2(b)]. The steps in the volume thermal expansion coefficient at T_1 and T_2 are $\Delta\alpha_1=1.5\times10^{-4}$ K^{-1} and $\Delta\alpha_2=4\times10^{-4}$ K^{-1}, respectively.

D. G_2PbI_4 structure

The G_2PbI_4 structure is built of two-dimensional corrugated sheets of the $(PbI_4)_n^{2-}$ polyanion perpendicular to [010], and of guanidinium cations occupying cavities within the polyanions and voids between the sheets, as shown in Fig. 4. These voids will be further referred to as ''cage'' and ''channel'' voids, respectively. The cage and channel cavities are approximately similar in shape and size, 6.3 Å along [y] and [z]. Phase III is monoclinic, space group $P2_1/n$ with

TABLE II. Atomic coordinates and equivalent isotropic displacement parameters ($Å^2$) for G_2PbI_4. U_{eq} is defined as one third of the trace of the orthogonalized U_{ij} tensor.

	x	y	z	U_{eq}
Pb(1)	−0.2568(5)	0.0849(3)	0.2491(8)	0.038(2)
I(1)	−0.0032(8)	0.0755(5)	0.3064(13)	0.053(3)
I(2)	0.2535(9)	0.0042(5)	0.0009(13)	0.049(3)
I(3)	−0.2198(11)	0.1591(5)	−0.0066(14)	0.067(4)
I(4)	−0.2596(9)	0.1676(5)	0.4777(13)	0.053(3)
Pb(2)	0.2449(5)	0.0890(2)	0.2574(8)	0.039(2)
I(5)	0.4960(8)	0.1024(5)	0.1996(12)	0.053(3)
I(6)	0.2913(9)	−0.0011(4)	0.4991(12)	0.048(3)
I(7)	0.2622(9)	0.1693(5)	0.4982(13)	0.057(3)
I(8)	0.2020(9)	0.1673(5)	0.0253(13)	0.055(3)
C(1)	0.002(4)	−0.063(3)	0.226(7)	0.06(5)
N(1)	0.003(7)	−0.058(6)	0.082(7)	0.09(6)
N(2)	−0.090(4)	−0.062(6)	0.293(11)	0.07(5)
N(3)	0.090(5)	−0.074(5)	0.299(10)	0.06(4)
C(2)	−0.010(5)	−0.235(2)	0.271(11)	0.09(6)
N(4)	0.059(6)	−0.260(3)	0.193(11)	0.18(7)
N(5)	−0.102(6)	−0.256(4)	0.302(12)	0.09(5)
N(6)	0.006(9)	−0.187(3)	0.300(13)	0.09(6)
C(3)	0.509(5)	−0.252(3)	0.166(14)	0.13(8)
N(7)	0.558(8)	−0.216(3)	0.098(12)	0.12(9)
N(8)	0.564(8)	−0.286(6)	0.240(13)	0.26(8)
N(9)	0.404(9)	−0.241(7)	0.212(29)	0.19(8)
C(4)	0.520(5)	−0.083(3)	0.262(10)	0.05(4)
N(10)	0.599(6)	−0.106(5)	0.201(12)	0.09(6)
N(11)	0.468(9)	−0.047(5)	0.189(11)	0.10(6)
N(12)	0.496(9)	−0.092(5)	0.399(11)	0.08(5)

two symmetry-independent G_2PbI_4 formula units; space group Pn was rejected in the R-factor test,[17] which was consistent with the absence of piroelectric effect. The monoclinic structure of phase III, with halved parameters a and b,

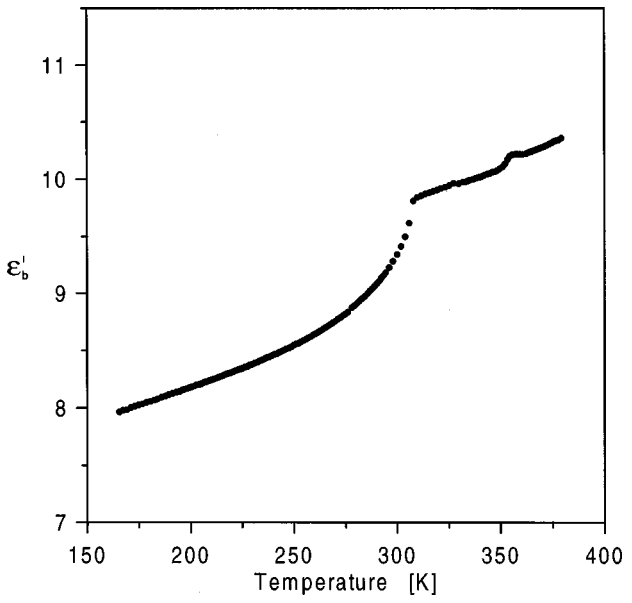

FIG. 3. Temperature dependence of a real part of dielectric constant measured for the G_2PbI_4 single crystals along [010].

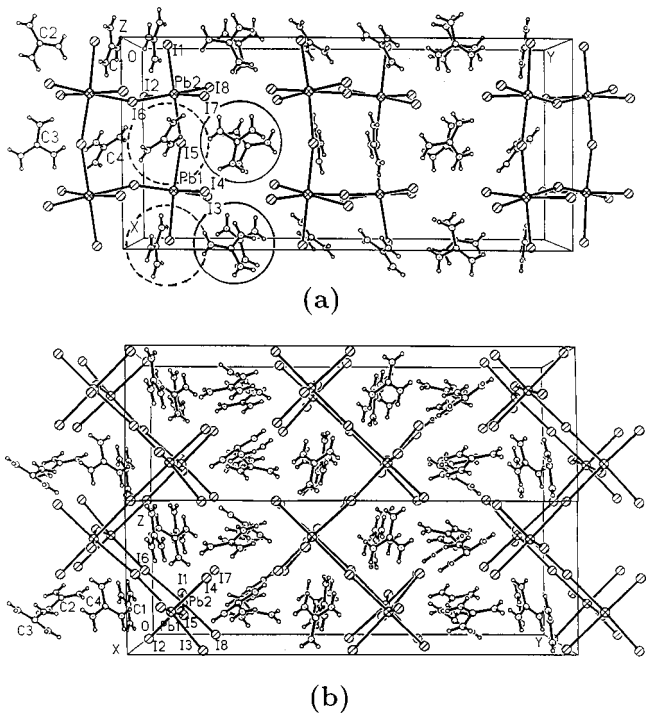

FIG. 4. The G_2PbI_4 crystal structure in phase III at 287 K viewed (a) down [001], and (b) down [100]. Two symmetry-independent channel voids, running along [001] and separating the polyanions are indicated with full-line circles in drawing (a); the central lines of the channel voids have approximate coordinates 0,1/4,z, and 1/2,1/4,z; the guanidinium cations lie at z coordinates close to 1/4 and 3/4 along these channels. The channel voids are perpendicular to drawing (a) and they are vertical in drawing (b). The approximate coordinates of two symmetry-independent cage voids, formed between the PbI_6 octahedra within the polyanion, are 0,1/12,3/4, and 1/2,1/12,3/4. Two cage voids are indicated by broken-line circles in drawing (a).

approximates orthorhombic space group $Pmcm$. This pseudosymmetry is lowered in phase III, to the quadruple unit-cell and to the centrosymmetric space group $P2_1/n$, due to tilts and small distortions of the PbI_6 octahedra, as well as due to misorientations of the guanidinium cations. The guanidinium cations are weak x-ray scatterers compared to much more strongly scattering Pb and I atoms. Consequently, the cations were located with difficulty and refined as rigid groups. More convincing observations doubling parameters a and b of the pseudosymmetric $Pmcm$ unit cell are distortions of the PbI_6 octahedra clearly visible in Fig. 4(a) and in the dimensions of the polyanion, listed in Table III.

IV. DISCUSSION

A. Ferroelastic phase transition at $T_2 = 307$ K

The reduction of the crystal symmetry from the orthorhombic to monoclinic system implies that two orientational states appear in low-temperature phase III. The crystal samples observed in the polarized light revealed domains with (001) and (100) walls, as expected for the $mmmF2/m$ species.[18] The appearance of the ferroelastic domains arises from spontaneous shear stress σ_{13}. In the microscopic scale the nonzero value of σ_{13} implies a distortion of the anionic

TABLE III. Bond lengths (Å) and angles (deg) for G_2PbI_4. Symmetry transformations used to generate equivalent atoms: [1], $-x,-y,-z$; [2], $x-1,y,z$; [3], $-x,-y,1-z$; [4], $x+1,y,z$.

Pb(1)-I(1)	3.300(12)	Pb(2)-I(1)	3.243(12)
Pb(1)-I(2 [3])	3.35(2)	Pb(2)-I(2)	3.31(2)
Pb(1)-I(3)	3.15(2)	Pb(2)-I(7)	3.13(2)
Pb(1)-I(4)	3.09(2)	Pb(2)-I(8)	3.070(14)
Pb(1)-I(5 [1])	3.233(12)	Pb(2)-I(5)	3.294(12)
Pb(1)-I(6 [2])	3.294(13)	Pb(2)-I(6)	3.362(14)
I(1)-Pb(1)-I(2 [3])	91.9(3)	I(1)-Pb(2)-I(2)	94.1(4)
I(1)-Pb(1)-I(3)	90.4(4)	I(1)-Pb(2)-I(5)	178.7(4)
I(1)-Pb(1)-I(4)	88.4(4)	I(1)-Pb(2)-I(6)	89.0(3)
I(1 [1])-Pb(1)-I(5)	175.9(4)	I(1)-Pb(2)-I(7)	91.8(4)
I(1)-Pb(1)-I(6 [2])	88.8(3)	I(1)-Pb(2)-I(8)	91.0(4)
I(2 [3])-Pb(1)-I(3)	86.1(4)	I(2)-Pb(2)-I(5)	84.8(3)
I(2 [3])-Pb(1)-I(4)	179.6(4)	I(2)-Pb(2)-I(6)	88.2(4)
I(2 [3])-Pb(1)-I(5 [1])	92.0(3)	I(2)-Pb(2)-I(7)	174.0(4)
I(2 [3])-Pb(1)-I(6 [2])	90.0(4)	I(2)-Pb(2)-I(8)	89.0(4)
I(3)-Pb(1)-I(4)	93.5(4)	I(5)-Pb(2)-I(6)	91.8(3)
I(3)-Pb(1)-I(5 [1])	87.9(4)	I(5)-Pb(2)-I(7)	89.3(4)
I(3)-Pb(1)-I(6 [2])	176.0(4)	I(5)-Pb(2)-I(8)	88.2(4)
I(4)-Pb(1)-I(5 [1])	88.0(4)	I(6)-Pb(2)-I(7)	91.1(4)
I(4)-Pb(1)-I(6 [2])	90.4(4)	I(6)-Pb(2)-I(8)	177.2(4)
I(5 [1])-Pb(1)-I(6 [2])	93.2(3)	I(7)-Pb(2)-I(8)	91.7(4)
Pb(1)-I(1)-Pb(2)	159.4(5)	Pb(1 [4])-I(5)-Pb(2)	156.9(5)
Pb(1 [3])-I(2)-Pb(2)	177.5(5)	Pb(1 [2])-I(6)-Pb(2)	161.8(4)

sublattice. Within one polyanionic layer, parallel to plane (010), the PbI_6 octahedra form two symmetry-independent zigzag chains along $[z]$, as shown in Fig. 4. The zigzag motif of the chains lie approximately in the (100) planes. The PbI_6 octahedra neighboring along $[x]$ are symmetry-independent. The nonzero σ_{13} induces nonorthogonality between a and c, corresponding to small translations of the zigzag chains along $[z]$ with respect to their neighbors. This is manifested by the monoclinic distortion of β, which is related to the spontaneous shear strain e_{13} according to the simple equation:[19]

$$e_{13}=\tan[(\beta-90°)/2]. \tag{1}$$

The temperature dependence of e_{13} is shown in Fig. 5(a).

Landau's mean-field approximation[20–22] was used to describe the temperature dependence of e_{13} and of the excess heat capacity. The free-energy expansion in the form

$$F=F_0+at\eta^2+b\eta^4+c\eta^6 \tag{2}$$

has been used for describing the transition at T_2, where F_0 denotes the free energy of the high-temperature (disordered) phase, and t is the reduced temperature: $t=(T-T_2)/T_2$. The temperature dependence of the order parameter resulting from Eq. (2) is:

$$\eta=A\left[\frac{(T^*-T)^{1/2}}{(T^*-T_2)^{1/2}}-1\right]^{1/2}, \tag{3}$$

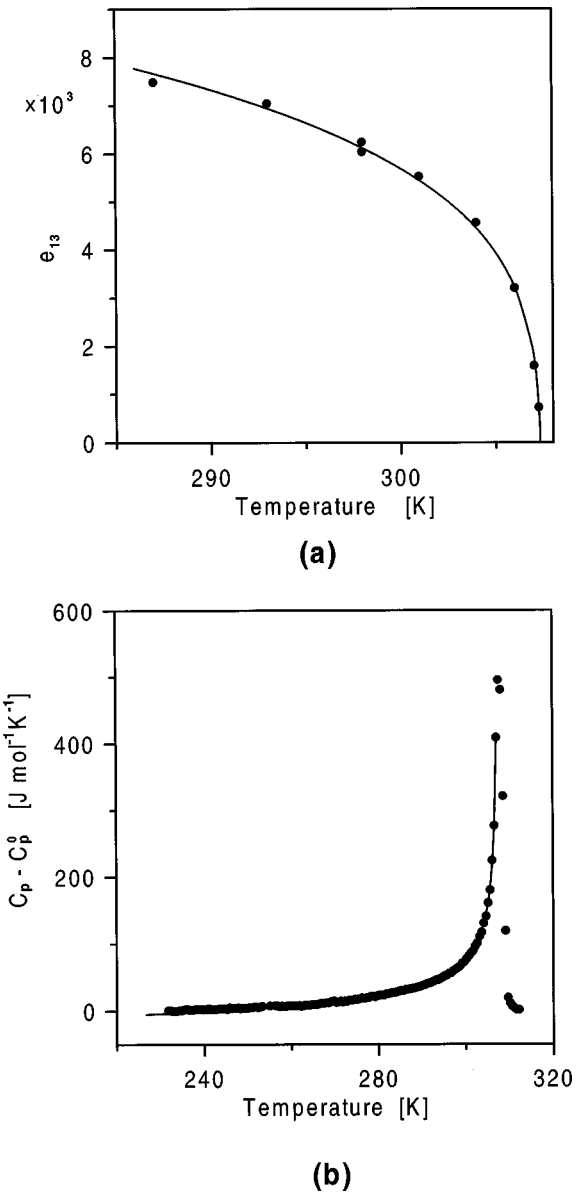

FIG. 5. Temperature dependencies (a) of the order parameter, spontaneous strain e_{13} and (b) of the excess heat capacity ($C_p-C_p^0$), where C_p^0 denotes the normal part of C_p. Solid lines show the functions fitted to these data according to Eqs. (3) and (5), respectively.

where $T^*=T_2+(b^2T_2/3ac)$, and $A=(b/3c)^{1/2}$.

The excess heat capacity can be approximated by the formula:

$$C_p-C_p^0=BT(T^*-T)^{-1/2}, \tag{4}$$

where $B=[a^3/(12cT_0^3)]^{1/2}$, and C_p^0 is the normal part of C_p. The experimental values of the order parameter e_{13} can be well described by Eq. (3), with the goodness-of-fit of 0.997, [Fig. 5(a)]. The values of parameters T^* and A obtained form the least-squares fit of the data to Eq. (3) are 307.70 K and 3.085, respectively. Equation (4) could be well fitted [goodness-of-fit 0.9994, see Fig. 5(b)] to the measured excess heat capacity after including an additional constant term B':

$$C_p - C_p^0 = BT(T^* - T)^{-1/2} + B'. \quad (5)$$

Parameters B and B' assume values 0.9844 $\mathrm{J\,K^{-3/2}\,mol^{-1}}$ and -29.8339 $\mathrm{J\,K^{-1}\,mol^{-1}}$; the value of parameter T^* obtained from Eq. (3) was applied. The negative value of parameter B' may be due to critical fluctuations close to the transition,[23] although it would require the exponent different from 0.5, or to the choice of C_p^0. However, these conclusions should be verified by more precise adiabatic-calorimetry measurements. It is possible that apart from the order parameter related to the spontaneous shear strain, yet another parameter related to ordering of the cations in the cage voids may be required in Landau's expansion of the crystal potential.

The appearance of nonzero e_{13} can be hardly explained only in terms of the anionic sublattice, without referring to its interactions with the cations or to the interactions between the cations. The triangular symmetry of the cations is incompatible with the rectangular shape of the voids (Fig. 4) and their interactions may lead to the monoclinic deformation of the polyanions. The iodine atoms vibrate most strongly perpendicular to their bonds to Pb, consistently with the so-called ''riding model'' of lighter atoms vibrating around a heavier atom to which they are chemically bonded.[24] It is apparent that higher temperatures increase the amplitudes of vibrations of the iodine atoms, and in this way they compress the contents of the voids. However, higher temperatures also enhance vibrations of the light and bulky guanidinium cations, which thus exert higher pressure on the walls of the voids. The process of compressing the voids is temperature sensitive, because the strongest vibrations of the iodine atoms are normal to their bonds to Pb. It is reasonable to assume that the terminal iodines I(3), I(4), I(7), and I(8) are most mobile, because their positions are stabilized only by one covalent bond to Pb. Therefore the volume of the cage voids decreases more strongly on the side of the terminal iodines, and consequently the guanidinium cations in the cage voids change their orientations with temperature. The temperature dependence of dielectric constant near T_2 (Fig. 3) reflects a change in polarity of the cation-anion system, which may result from the increased mobility of the cations. This process cannot be related to the reorientations of the guanidinium cations about their C_3 axes occurring in phase III,[12] as the cation does not have a permanent dipole moment. It is plausible that the changes in ε' are related to other types of motion of the cations: their hopping between different positions in the voids, or the tumbling motion of one of two different guanidinium cations postulated on the basis of ^{1}H NMR second moment measurements.[12] Molecular motions of this kind would produce fluctuations of the local dipole moments, which could contribute both to the real and imaginary parts of dielectric constant. This is consistent with the high entropy of the transition at T_2. The temperature dependence of the lattice parameters and the pressure dependence of the structure (see Sec. IV C) strongly suggest that these are the guanidinium cations in the cage voids, which become activated. The disordered cations occupy larger volume and their interactions with the atoms forming the walls of the cage voids are effectively more uniform and stronger, leading to an increase in the distance between the zigzag chains along $[x]$ (see Fig. 4). When temperature is lowered below T_2, the onset of ordering of the cations is accompanied by the anomalous shortening of a. The ordering of the cations also differentiates their interactions with the walls of the cage voids, and distorts the anionic sublattice (compare Figs. 4 and 6). Thus, both processes of cationic disordering and of the shear deformation are coupled.

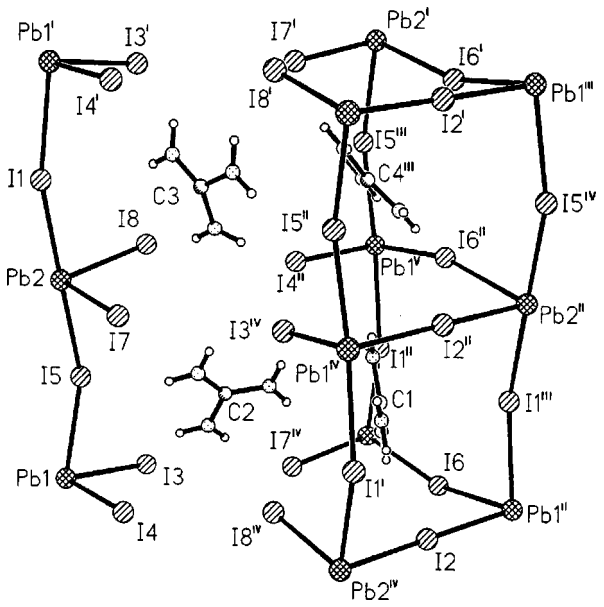

FIG. 6. Four symmetry-independent guanidinium cations enclosed in the neighboring channel (left) and cage (right) voids in phase III of G_2PbI_4.

B. Phase transition at $T_1 = 356$ K

The phase transition between phases II and I is associated with a relatively small entropy change, does not affect noticeably the cations dynamics[12] and is poorly manifested in dielectric properties of the crystal (see Fig. 3). Thus the mechanism of the transition at T_1 can mainly involve the distortions in the anionic sublattice. The most flexible fragments of the polyanionic layers are the Pb-I-Pb bonds, so it is plausible that above T_1 the Pb(2)-*I*(6)-Pb(1′) and Pb(1)-I(5)-Pb(2) angles straighten (atom labeling of phase III has been adopted for this discussion, and the prime denotes the atom transformed according to the symmetry code: $1-x,-y,1-z$). Indeed, Fig. 2 shows that the largest anomaly in the thermal expansion of phase II is observed along $[x]$. This anomaly can be directly connected with the changes in the Pb(1)-I(5)-Pb(2) and Pb(2)-I(6)-Pb(1′) angles. Due to their straightening at T_1 an anomalous lengthening of a is observed, and this parameter approximates the sum of the Pb-I bond length measured in phase III (see Fig. 4). Moreover, the tilts of the PbI_6 octahedra, resulting from the nonlinear Pb-I-Pb angles, are the main distortions responsible for doubling unit-cell dimensions a and b in phase II, when the guanidinium cations are disordered. Above T_1 the translational symmetry of the crystal along $[x]$ and $[y]$ is halved, which has been confirmed by the single-crystal x-ray and powder neutron-diffraction studies.[25] Due to these changes octahedra $Pb(1)I_6$ and $Pb(2)I_6$, symmetry independent in phase III, become symmetry related. It follows from the reduction of the unit-cell volume in phase I that the PbI_6

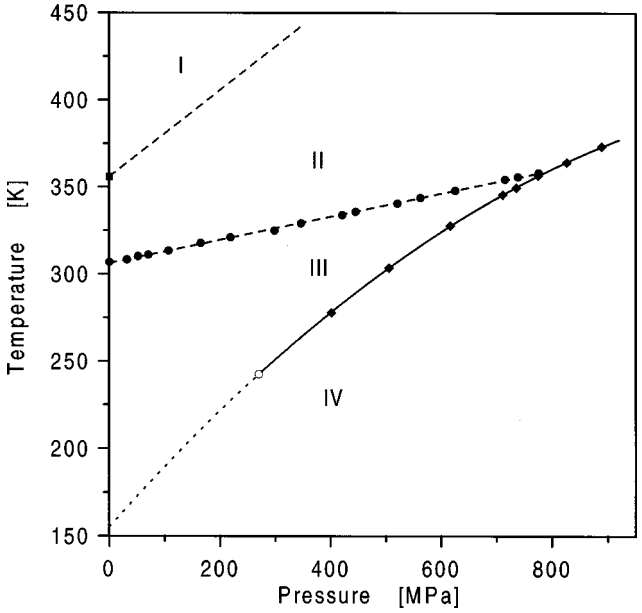

FIG. 7. Phase diagram of G_2PbI_4. The solid line denotes the first-order phase transition, the dashed lines denote second-order phase transitions, and the dotted line extrapolates the transition between phases III and IV to zero pressure (see the text). The small open circle marks the critical point estimated from the $\Delta S_3(p,T)$ function.

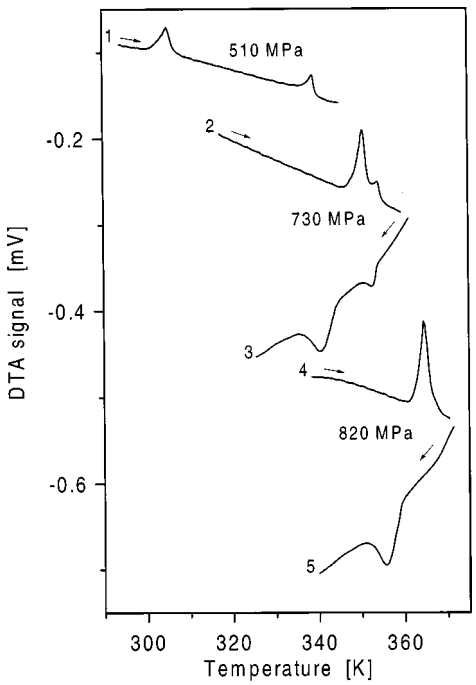

FIG. 8. Exemplary DTA runs on heating and cooling the G_2PbI_4 sample, as indicated by the arrows, for the pressure of 510 MPa, much lower than the triple point at 780 MPa, close to the triple point (730 MPa), and above it (820 MPa).

octahedron is located on a point-symmetry element, which imposes geometrical constrains on the PbI_6 dimensions. This symmetry requirement modifies the coordination of the Pb atom. This results in the color change of the G_2PbI_4 crystals from deep yellow to light red when the temperature increases above T_1. This is connected with the shift of fundamental absorption edge of the crystal, and confirms that displacements of the iodine atoms, as well as modifications of the electronic structure of the PbI_6 octahedra take place. Analogous dependence of the fundamental absorption edge and the anionic geometry was observed in alkaline halide crystals.[26,27]

C. *p*-*T* phase diagram of G_2PbI_4

Owing to minute changes in dielectric permittivity and thermal properties of G_2PbI_4 at T_1, transition between phases II and I is hardly detectable by dielectric or calorimetric methods under high pressure. However, for continuous phase transitions the pressure dependence of the transition temperature can be estimated from Ehrenfest's relation:

$$dT/dp = TV\Delta\alpha/\Delta C_p, \tag{6}$$

where $\Delta\alpha$ and ΔC_p are changes in specific-volume thermal-expansion coefficient and in specific heat, respectively. Having determined $\Delta\alpha_1$ and V from dilatometric measurements and ΔC_{p1} from DSC measurements, the pressure coefficient $dT_1/dp = 0.249\ \mathrm{K\,MPa^{-1}}$ was calculated. The boundary between phases I and II can be approximated by the linear equation

$$T_1(p) = 356 + 0.249p, \tag{7}$$

indicated by a dashed line in Fig. 7. The same procedure applied to the transition between phases II and III gives the pressure coefficient $dT_2/dp = 0.062\ \mathrm{K\,MPa^{-1}}$, which well agrees with the experimentally determined value of $0.067\ \mathrm{K\,MPa^{-1}}$.

The most striking feature of this phase diagram is a pressure-induced transition from phase III to a new phase denoted IV. This transition has a clearly first-order character manifested by temperature hysteresis of about 3 K, as seen from the cooling and heating DTA runs shown in Fig. 8. It becomes hardly detectable at lower pressures, when the transition temperature T_3 decreases below 270 K. At ambient pressure no anomaly in calorimetric or dielectric measurements could be detected about 155 K extrapolated for the zero pressure, as indicated by the dotted line in Fig. 7. Also no anomalous changes in lattice constants nor in the symmetry of the crystal could be found by powder neutron-diffraction measurements.[25] These results can be explained by the isostructural character of the phase transition between phases III and IV, and by the existence of a critical point.

The boundary between phases III and IV is evidently nonlinear. The pressure dependence of the transition temperature is described for first-order phase transitions by the Claussius-Clapeyron equation:

$$dT/dp = \Delta V/\Delta S, \tag{8}$$

where ΔV and ΔS are the volume and entropy changes at the transition temperature, respectively. According to Eq. (8), the nonlinearity in $T_3(p)$ may arise of the changes in ΔS_3 or/and in ΔV_3 induced by pressure. To clarify this, the changes in transition entropies ΔS_2 and ΔS_3 were estimated by integrating the anomalous parts of the DTA signals according to the formula

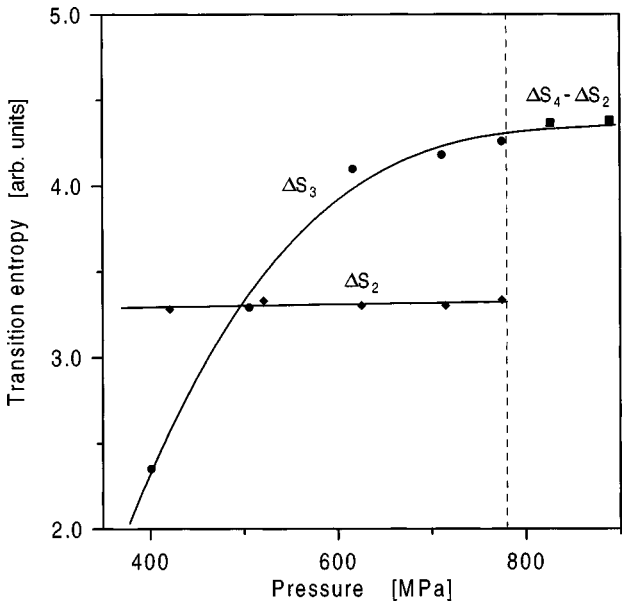

FIG. 9. Pressure dependence of the entropies of transitions between phases III-II (ΔS_2), between phases IV-III (ΔS_3), and IV-II (ΔS_4) in G_2PbI_4. The latter dependence is shown in the form of (ΔS_4-ΔS_2) to show the relationship between ΔS_4 and the sum ($\Delta S_3 + \Delta S_2$). The vertical dashed line indicates the pressure of the triple point.

$$\Delta S = \int \frac{S - S_b}{T} dT, \tag{9}$$

where S and S_b denote the DTA signal and the baseline, respectively. For the measurements at pressures close to the triple point at 358 K and 780 MPa, common for phases II, III and IV, where the anomalies overlap (see Fig. 8), a constant contribution of ΔS_2 was assumed. In Fig. 9, the entropy of the transition between phases IV and II, ΔS_4, is represented by the quantity ΔS_4-ΔS_2, illustrating that near the triple point ΔS_4 approximates the sum of ΔS_3 and ΔS_2. As can be seen in Fig. 9, in the range of pressures from 300 MPa to the triple point, the transition entropy ΔS_2 is almost constant, while ΔS_3 increases strongly with increasing pressure. The pressure dependence of ΔS_3 is reflected in the nonlinear evolution of T_3 with pressure. It is evident from the comparison of the values of ΔS_2 and ΔS_3 that elevated pressures induce a new type of disorder in the G_2PbI_4 structure. A simple extrapolation of ΔS_3 to lower pressures proves that ΔS_3 becomes zero at a critical point about 245 K and 270 MPa, indicating that this disordering process disappears. The most pressure-susceptible elements of the G_2PbI_4 structure (Fig. 4) are the channel voids separating the polyanionic layers: at elevated pressures the channel voids may collapse when the guanidinium cations are squeezed to a more closely packed configuration. On the other hand, the rise of the transition entropy ΔS_3 suggests that number of sites occupied by the cations in the channel voids increases with pressure. Thus, the pressure modifies the potential function of the cations in the voids. The pressure-induced changes are strictly related to the anisotropy of the G_2PbI_4 structure. Most importantly, up to the triple point the guanidinium cations in the channel and cage voids behave to a large extent independently: the elevated pressures mainly affect the disordering of the cations occupying the channel voids, and do not disturb the transition between phases II and III connected to disordering of the cations occupying the cage voids (see Sec. IV A). Above the triple point the interplay between the cations in adjacent voids becomes prominent and their dynamics strongly correlated, which results in the first-order phase transition between phases II and IV.

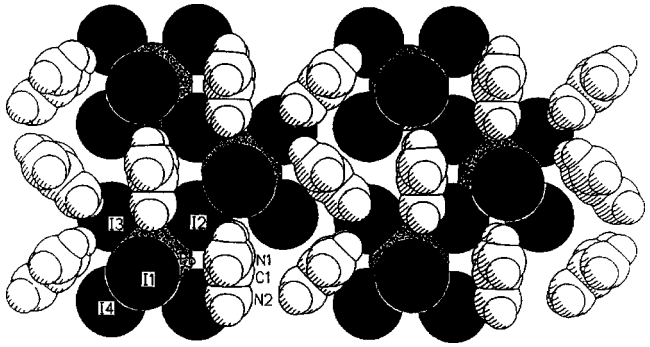

FIG. 10. Space-filling drawing of the G_2PbI_4 structure viewed down [100] illustrating a possible configuration of guanidinium cations in the voids. The black circles denote iodines, and the dotted circles denote Pb atoms.

D. Cooperativity in the G_2PbI_4 structure

It is apparent that size and shape of the voids influence the orientation of the cations. As can be seen from Fig. 6 and Table III, the tilts and deformations of the octahedra considerably influence the shape of the voids. The iodine atoms are mainly responsible for interactions between the cations and the walls of the voids, and in this way with the anionic sublattice (see Fig. 10). The tilts of the octahedra differentiate the shape of the neighboring voids along $[x]$, which in this way become symmetry independent below T_1 (see Fig. 6). The iodine atoms protrude toward inside or to outside of the voids, and the cations appropriately change their orientations to minimize interactions with the iodines. Moreover, orientations of the cations are limited by their interactions between the cage and channel voids, because the double void is about 9 Å in length (as estimated from the coordinates and the van der Waals radii of the iodine atoms, see Figs. 6 and 10), while the length of the guanidinium cation measured along one of its C-N bonds is 5.5 Å. Consequently, at least one of the cations has to be tilted with respect to the $[y]$ axis. The same reasoning applies to the mutual orientation of the guanidinium cations in the channel voids along $[z]$. The width of one channel void along $[z]$ of 4.65 Å does not allow all the cations in the channel void to align along this direction, with their plane perpendicular to $[y]$. As can be seen from Fig. 4, the cations assume orientations inclined to the crystallographic directions in phase III. Another possible arrangement illustrated in Fig. 10 shows that the size of the cage voids allows that the cations inside may be perpendicular to $[y]$. In this space filling drawing also the voids formed by the polyanions and the contact walls between the neighboring voids are clearly visible. The restrictions resulting from the sizes of the cation and voids does not allow the system to attain the high-$Pmcm$ symmetry approximated by the anionic structure, unless the cations are disordered. This

can be attained by subtle structural changes induced to the crystal by varying thermodynamic conditions, changing the available void space, as well as the tilts of the PbI_6 octahedra, and by providing kinetic energy to the cations, which increases the number of energetic states in the lattice. The contacts between the cations in the neighboring voids are transmitted not only via the distortions of the polyanionic lattice, but the cations can also interact directly through the gaps joining the cage and channel voids. These gaps are somewhat wider between cage and channel voids than between the segments of the channel voids: the average I-I distances in the cage-to-channel gaps are 4.87 Å along $[z]$ and 6.25 Å along $[x]$, while the average I-I distances in the gaps between channel voids are 4.57 Å along $[y]$ and 6.12 Å along $[x]$. It is plausible that the role of direct intercationic interactions prevail in the high-pressure phase: the cations in the channel voids, most susceptible to pressures, may change their arrangement from zigzag-like (see Fig. 10) to parallel, or they may partly penetrate the cage voids. However, further high-pressure structural studies are required to clarify the role of the direct intercationic interactions.

V. CONCLUSIONS

The characteristic feature of the G_2PbI_4 crystals is the pseudosymmetric polyanionic substructure with the system of voids containing guanidinium cations. The orientation of the cations is strongly correlated along the channels, and between the channel and cage voids. In this respect the G_2PbI_4 crystal presents a potentially cation-shape and size-tunable system undergoing a series of phase transitions induced by changes in orientational configurations of the cations in the voids. The adjustment of the void and cation sizes pertains to the most fundamental concepts of crystal-chemistry formulated by Goldschmidt, and developed by Pauling and others. The G_2PbI_4 structure-property relations depend on the size of the constituent units, but also on their shape and orientation. In this respect G_2PbI_4 differs from simple ionic crystals, like perovskites, where only the size of spherical ions is the main factor governing the crystal structures and properties. Like in perovskites, small distortions of the ionic arrangement lower the symmetry of the highly pseudosymmetric lattices.[28] In this respect the anionic sublattice of G_2PbI_4 is strikingly similar to the polyanions of the two-dimensional ferroelectrics of the $BaMF_4$ family.[8] Moreover, due to the specific features of the organic cations, the G_2PbI_4 crystals are much more susceptible to thermodynamic conditions than their purely inorganic counterparts: for example the $BaMnF_4$ and $BaCdF_4$ crystals do not undergo transitions to their prototypical phases, as they melt at lower temperatures. The phase transitions and lattice instabilities in these materials are induced exclusively by rotations of the octahedra.[10] Two types of voids and nonspherical cations induce new types of cooperativity in G_2PbI_4, and the phase diagram of this crystal acquires new interesting features such as pressure-induced phase transition due to cationic disorder, as well as the critical and triple points. The intriguing properties of the G_2PbI_4 crystals, multidimensional cooperativity, and correlation lengths, pressure-induced disordering, color changes, and phase transitions can be conveniently studied by directly observing the cationic and polyanionic interactions and structural distortions. For the full description of the G_2PbI_4 transformations more detailed information about behavior of the guanidinium cations and of the polyanions in the function of temperature and pressure is required. Therefore further high-pressure and neutron-diffraction studies on single G_2PbI_4 crystals have been undertaken.

ACKNOWLEDGMENTS

We gratefully acknowledge a partial support from the Interdisciplinary Grant No. P2-6 for this project. The authors thank Dr. S. Mielcarek, of the Faculty of Physics at the Adam Mickiewicz University, for the DSC measurements, Dr. G. J. McIntire, of Institute Laue-Langevin in Grenoble, for detecting the quadruple unit-cell volumes of phases III and II, and Dr. A. Hoser, of the Hahn-Meitner Institute in Berlin, for his assistance in performing the neutron-diffraction powder experiments.

[1] T. Ishihara, J. Takahashi, and T. Goto, Solid State Commun. **69**, 933 (1989).
[2] M. Hirasawa, T. Ishihara, T. Goto, S. Sasaki, K. Uchida, and N. Miura, Solid State Commun. **86**, 479 (1993).
[3] X. Hong, T. Ishihara, and A.V. Nurmikko, Phys. Rev. B **45**, 6961 (1992).
[4] D.B. Mitzl, C.A. Feild, W.T.A. Harrison, and A.M. Guloy, Nature (London) **369**, 467 (1994).
[5] R. Kind, S. Pleško, H. Arend, R. Blinc, B. Žekš, J. Seliger, B. Ložar, J. Slak, A. Levstic, C. Filipič, V. Žagar, G. Lahajnar, F. Mila, and G. Chapuis, J. Chem. Phys. **71**, 2118 (1979).
[6] D.M. Hatch, H.T. Stokes, K.S. Aleksandrov, and S.V. Misyul, Phys. Rev. B **39**, 9282 (1989).
[7] K.S. Aleksandrov and J. Bartolomé, J. Phys.: Condens. Matter **6**, 8219 (1994).
[8] E.T. Keve, S.C. Abrahams, and J.L. Berstein, J. Chem. Phys. **51**, 4928 (1969).
[9] R. Almairac, H.N. Bordallo, A. Bulou, J. Nouet, and R. Currat, Phys. Rev. B **55**, 8249 (1997).
[10] Ph. Sciau, J. Lapasset, D. Grebille, and J.F. Berar, Acta Crystallogr., Sect. B: Struct. Sci. **44**, 108 (1988).
[11] M. Szafrański, Thermochim. Acta **307**, 177 (1997).
[12] M. Grottel, M. Szafrański, and Z. Pająk, Z. Naturforsch., A: Phys. Sci. **52**, 783 (1997).
[13] M. Szafrański, P. Czarnecki, A. Katrusiak, and S. Habryto, Solid State Commun. **82**, 277 (1992).
[14] A. Katrusiak and M. Szafrański, Acta Crystallogr., Sect. C: Cryst. Struct. Commun. **50**, 1161 (1994).
[15] A. Katrusiak and M. Szafrański, J. Mol. Struct. **378**, 205 (1996) .
[16] G. M. Sheldrick, SHELXL-93, program for crystal structure refinement (University of Göttingen, Göttingen, 1993).
[17] W. C. Hamilton, *International Tables for X-ray Crystallography* (Kynoch, Birmingham, 1974), Vol. IV.
[18] J. Sapriel, Phys. Rev. B **12**, 5128 (1975).

[19] J. F. Nye, *Physical Properties of Crystals. Their Representation by Tensors and Matrices* (Clarendon, Oxford, 1957).
[20] L. D. Landau and E. M. Lifshitz, *Statistical Physics* (Pergamon, Oxford, 1969).
[21] B. A. Strukov and A. P. Levaniuk, *Fizicheskie Osnovy Segneto-elektricheskih Iavlenii v Kristalah* (Izdatelstvo Nauka, Moscow, 1983), p. 72.
[22] J.-C. Toledano and P. Toledano, *The Landau Theory of Phase Transitions* (World Scientific, Singapore, 1987).
[23] J.F. Nicoll and F.C. Albright, Phys. Rev. B **34**, 1991 (1986).
[24] D.W.J. Cruickshank, Acta Crystallogr. **9**, 747 (1956).
[25] M. Szafrański and A. Hoser, in *Berlin Neutron Scattering Center Experimental Reports, 1996*, edited by Y. Kirschbaum, H. Waldmann, and R. Michaelsen (Hahn-Meitner Institut, Berlin, 1997), p. 144.
[26] M. Szafrański and M. Koralewski, Acta Phys. Pol. A **75**, 705 (1989).
[27] M. Szafrański and K. Ståhl, Z. Kristallogr. **209**, 491 (1994).
[28] A.M. Glazer, Acta Crystallogr., Sect. B: Struct. Crystallogr. Cryst. Chem. **28**, 3384 (1970); A. Katrusiak and A. Ratuszna, Solid State Commun. **84**, 435 (1992); R. Ramirez, H. Vincent, R.J. Nelmes, and A. Katrusiak, *ibid.* **77**, 927 (1991); N.W. Thomas, Acta Crystallogr., Sect. B: Struct. Sci. **54**, 585 (1998).